Research article

Innovative eco-friendly methyl orange removal: Mechanism, kinetic, and thermodynamic study using starch cryogel-integrated mesoporous silica nanoparticles

Tarawee Taweekarn [a], Worawit Wongniramaikul [a], Wilasinee Sriprom [a], Wadcharawadee Limsakul [a], Chanadda Phawachalotorn [b], Aree Choodum [a,*]

[a] *Integrated Science and Technology Research Center, Faculty of Technology and Environment, Prince of Songkla University, Phuket Campus, Kathu, Phuket, 83120, Thailand*
[b] *King Mongkut's Institute of Technology Ladkrabang, Prince of Chumphon Campus, Chumphon, 86160, Thailand*

ARTICLE INFO

ABSTRACT

This study introduces a novel, eco−friendly composite, uncalcined mesoporous silica nanoparticles incorporated into a starch cryogel (MSNs-Cry), designed for the effective removal of methyl orange (MO) from water. MSNs−Cry integrates uncalcined mesoporous silica nanoparticles (MSNs) within a starch cryogel network, leveraging the high adsorption capacity of MSNs. The composite achieved a maximum adsorption capacity of 18.98 mg g^{-1} and demonstrated high removal efficiencies of 99.00 % ± 0.21 % in synthetic water (10 mg L^{-1} MO) and 92.77 % ± 1.76 % in real wastewater containing 0.43 mg L^{-1} MO. The Langmuir isotherm model provided a superior fit (R^2 = 0.9930) compared to the Freundlich model (R^2 = 0.9180), and the adsorption kinetics followed a pseudo−second−order model (R^2 = 0.9917). The primary adsorption mechanisms included electrostatic attraction, hydrophobic interactions, and hydrogen bonding. The process was endothermic (ΔH° = 31.3 kJ mol^{-1}), spontaneous, and more favorable at higher temperatures (ΔG° = −34.2 to −38.6 kJ mol^{-1} at 298–318 K). In the presence of sodium silicate at 13.1 times the MO concentration, removal efficiency drops by 35.77 %, and with sodium sulfate and urea at 100 times the MO concentration, it decreases by 8.65 %. Despite these challenges, MSNs−Cry effectively removes MO in the presence of the anionic dye Congo Red and metal ions, demonstrating its selective adsorption capabilities. The tablet form of MSNs−Cry prevents the loss of uncalcined MSNs, mitigating potential environmental and operational impacts. Additionally, the composite's effectiveness at a natural pH of 6.65 eliminates the need for pH adjustment, offering a cost−effective solution for real−world applications. This study establishes MSNs−Cry as a promising material for sustainable water purification.

1. Introduction

Methyl orange (MO) is one of the anionic dyes commonly used in the textile and paper industries and is frequently discharged into water bodies [1–3]. Due to its complex aromatic molecular structure, this organic dye can reduce the permeability of sunlight, thereby slowing the photosynthetic activity of aquatic plants [4,5]. This disruption in the aquatic environment leads to a decline in

---

* Corresponding author.
   E-mail address: aree.c@phuket.psu.ac.th (A. Choodum).

biodiversity. Additionally, MO is stable to light, heat, and oxidizing agents, leading to its low biodegradability [1,3–5]. Conventional wastewater treatment processes, such as aeration in municipal wastewater treatment systems, often fail to effectively remove it [5–7]. Consequently, MO exacerbates environmental pollution, presenting a significant challenge to the scientific community to develop effective removal techniques.

Numerous studies have been conducted to develop various methods for the removal of MO from solutions, including advanced oxidation processes [8,9], electrochemical degradation [10,11], photocatalytic degradation [12–14], and chemical reduction [15]. However, these methods suffer from limited effectiveness due to the properties of MO and the drawbacks of the techniques, such as high operational costs and the complexity of time−consuming operations [3,16]. Compared to the methods mentioned earlier, adsorption is more favorable due to its high effectiveness, byproduct−free nature, straightforward design and operation, resistance to toxicants, and low operational costs [3,17]. Recently, the performance of various adsorbents for MO adsorption, as reported in over 240 published works from 2016 to 2021, has been reviewed and classified into seven groups: activated carbon, biosorbents, biochar, clays and minerals, nanoparticles, polymers and resins, and composites [3]. The authors concluded that composites were the most frequently used (42.9 %), with nanoparticles (41.2 %) and polymers (28.2 %) being the most common compositions in the preparation of composite adsorbents for MO [3]. This is due to the flexibility of nanoparticles, which can integrate into the matrices of other materials due to their small size, and the ability of polymers to act as effective matrices for immobilizing other composite compositions [3]. Among the nanoparticles reported in the literature, mesoporous silica has shown the highest maximum removal capacity (Q_{max}) with high removal efficiency (%RE)—1000 mg g^{-1} and 92.0 % for MCM−41 [18] and 769.23 mg g^{-1} for MCM−48 [2]. This material has a large surface area, uniform pore size, and is easily modifiable with low toxicity [2,19,20]. These properties have led to increased applications in various fields, such as industrial processes, biosensing, and adsorption, including MO removal [2,20]. Mesoporous silica can be prepared from various silica sources, including tetraethyl orthosilicate (TEOS) [2], bamboo leaf ash [20], and banana peel ash [21]. Although Q_{max} was not reported for mesoporous silica synthesized from bamboo leaf ash and banana peel ash, their MO removal efficiencies were higher than 91.1 % [20] and 92.48 % [21], respectively. In contrast, mesoporous silica synthesized from TEOS has a reported removal capacity of 769.23 mg g^{-1} [2]. These materials perform best in acidic conditions (pH 2 to 3) [2,20,21]. Mesoporous silica can be combined with other materials to impart specific characteristics. For example, it can be composited with magnetic Fe$_2$O$_3$ nanoparticles to allow easier separation from the liquid phase using an external magnetic field, though this can lower the removal capacity from 1000–500 mg g^{-1} [18]. Additionally, it can be modified with agents such as poly(dia-llyldimethylammonium chloride) to increase its selectivity for MO [2]. However, all publications related to the application of mesoporous silica nanoparticles focus on developing adsorbents in the form of small particles, particularly nanocomposites. Although these nanocomposite materials provide high removal efficiency due to their larger surface area and more active sites, the loss of these particles during operation can negatively affect both the operating system and the environment [19,22,23]. To address this issue, some nanocomposites have immobilized nanomaterials within a polymeric matrix, particularly in the form of beads. For example, chitosan−Fe(OH)$_3$ beads, where Fe(OH)$_3$ is immobilized into chitosan, can remove MO with a Q_{max} of 314.45 mg g^{-1}. This method also addresses the challenge of separating powdery Fe(OH)$_3$ particles from the adsorption solutions [24]. However, commercial chitosan is quite expensive, whereas starch is much cheaper and offers several advantages, including wide availability, complete compostability, renewable nature, and nontoxicity [19,23,25,26]. The incorporation of starch with multi−walled carbon nanotubes (MWCNTs) has been reported to increase the distribution of the composite in aqueous solutions [26]. This enhancement improves the contact surface between the MWCNTs and MO molecules, reduces the aggregation of MWCNTs, and facilitates the diffusion of MO molecules to the surface of the MWCNTs [26]. Thus, the incorporation of mesoporous silica nanoparticles within a starch matrix may offer an attractive and advantageous alternative for MO removal. This approach could also contribute valuable scientific insights in the field of greener nanocomposites.

The aim of this study was to develop a novel and environmentally friendly composite material based on mesoporous silica nanoparticles to minimize the loss of active materials during MO removal process. Uncalcined mesoporous silica nanoparticles (uncalcined MSNs) were incorporated into a starch cryogel matrix to form a monolithic composite rod (MSNs−Cry). This rod can be cut into specified lengths for use in MO removal, either as a tablet or in a column. It is expected that MSNs−Cry will not only reduce the loss and aggregation of uncalcined MSNs but also be applicable for future continuous flow systems. Uncalcined MSNs were prepared using cetyltrimethylammonium bromide (CTAB) as a surfactant template and TEOS as the silica source. Since CTAB was not removed by calcination during preparation, it is expected to support a positively charged surface, which would electrostatically attract anionic MO during adsorption experiments, thus facilitating MO adsorption on the composite. Additionally, the hydroxy groups on both uncalcined MSNs and the starch network could synergistically support the electrostatic attraction of anionic MO, as well as hydrogen bonding. By avoiding the calcination process, the use of uncalcined MSNs not only conserves energy but also aligns with the principles of green chemistry. The prepared MSNs−Cry was characterized, and its adsorption mechanism, isotherms, kinetics, and thermodynamics were reported using synthetic water in a batch system. Furthermore, the removal of MO from a real wastewater sample was tested to evaluate the potential of MSNs−Cry for applicability in water treatment processes.

2. Materials and methods

The chemicals and materials used in this work are described in Supplementary Materials S1, while the instruments for characterization of the prepared materials are described in Supplementary Materials S2. All equations used in this work for both the adsorption experiments and theoretical models are summarized in Supplementary Materials Table S1. All experiments were performed in triplicate to ensure precision, and daily recalibration of the spectrophotometer was conducted to verify the accuracy of the quantitative analysis of MO concentration.

2.1. Preparation of MSNs−Cry

Uncalcined MSNs were prepared using a modified procedure from previous reports [27,28], as detailed in Supplementary Materials S3. MSNs−Cry were prepared by adding uncalcined MSNs (0.40–4.00 g) to a starch gel precursor (80.00 g) prepared according to procedures outlined in prior studies [19,23,25]. The mixture of starch gel and uncalcined MSNs was then filled into a 50 mL plastic syringe, where the monolithic MSNs−Cry rod was formed using the freeze and thaw method [19,23,25], as described in Supplementary Materials S3. The resulting MSNs−Cry rod was cut into shorter tablets measuring 0.25 cm in length for batch adsorption experiments.

2.2. Batch adsorption study for MO

Batch adsorption study was performed using standard MO solution which was prepared by diluting a stock solution of 1000 mg L^{-1} MO to get various concentrations (1−50 mg L^{-1}). The adsorption experiments were achieved using 300 mL standard MO solution at the natural solution pH (without pH adjusting = pH 6.65) at room temperature (25 °C) under magnetic stirrer. All solutions were collected at designable interval contact times, filtered through a cellulose acetate membrane (0.20 μm), and analyzed using spectrophotometer at λ_{max} 465 nm [29,30]. The adsorption conditions for optimization and batch experiment were based on preliminary studied results as followed: adsorbent doses of MSNs−Cry were optimized before using in adsorption studies by adding 0.35 g of MSNs−Cry (0.5, 1.0, 2.5, 5.0 % w/w) into 10 mg L^{-1} MO solution. The MO solutions were stirred at room temperature for 2 h. The percentage removal efficiency (%RE) of MO was calculated using Equation (1). The adsorption capacity of MO (concentration of adsorbed MO at equilibrium), Q_e (mg g^{-1}) was calculated using Equation (2).

$$Removal\ of\ MO\ (\%RE) = \frac{(C_0 - C_e)}{C_0} \times 100 \qquad (1)$$

where C_0 is the initial concentration and C_e is the equilibrium concentration of MO (mg L^{-1}). Each study was determined for three replicates where the average of these data was plotted or used to establish relationships.

$$Q_e = \frac{(C_0 - C_e)V}{m} \qquad (2)$$

where Q_e is the adsorbed capacity per unit mass at any time (mg g^{-1}), m is the dry weight of adsorbents (g) and V is the volume of the solution (L).
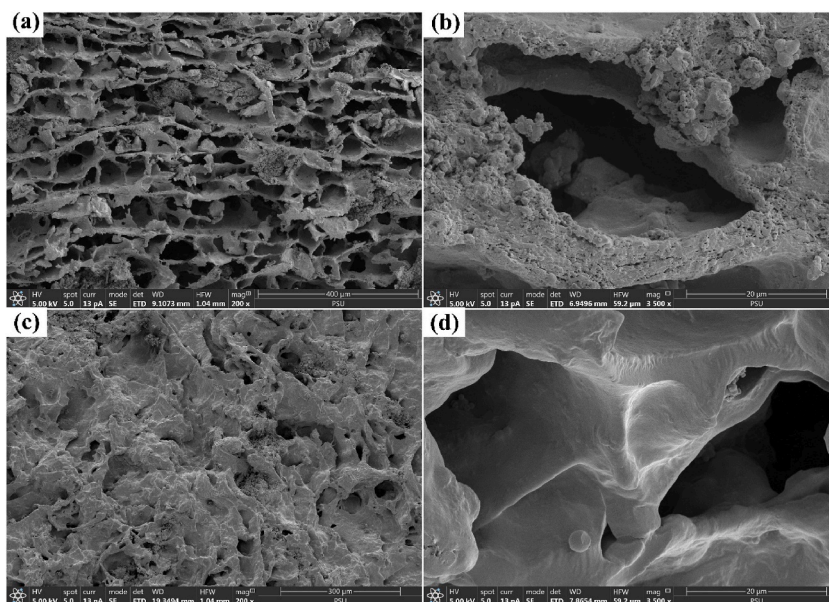

Fig. 1. Scanning electron micrographs of MSNs−Cry (a, b) before and (c, d) after MO adsorption, with magnifications of (a, c) 200X and (b, d) 3,500X.

3. Results and discussion

3.1. Characterization of MSNs−Cry

A novel monolithic composite rod, MSNs−Cry, was successfully developed for MO removal. Preliminary studies indicated that uncalcined MSNs achieved a higher MO removal efficiency (99.78 % ± 0.23 %) compared to calcined MSNs (5.65 % ± 0.23 %). This improved performance is likely due to the CTAB present in the uncalcined MSNs, which creates a positively charged surface that electrostatically attracts the anionic MO during adsorption, thereby enhancing MO removal. As a result, uncalcined MSNs were incorporated into a starch cryogel to produce the MSNs−Cry rod, optimizing its efficiency for MO removal. The particle size distribution of uncalcined MSNs, analyzed using a laser diffraction particle size analyzer, is shown in Supplementary Material S2, revealing a broad size range. Uncalcined MSNs contained particles ranging from 1 to 50 μm, similar to those reported for SBA-15 and SBA-16 (2–50 μm) in the literature [31]. The median of particle distribution (d_{50}) of uncalcined MSNs was 11.82 μm (Supplementary Materials Table S2), indicating that 50 % of the particles were smaller than 11.82 μm and 50 % were larger. After incorporation with starch cryogel to form MSNs−Cry, the particle size increased, ranging from 5 to 1000 μm, with a d_{50} value of 392.1 μm. It is important to note that MSNs−Cry typically exists in the form of a monolithic rod (a single rod rather than individual particles), so the reported particle size may depend on the crushing method used during analysis.

The morphology of MSNs−Cry (Fig. 1a−b) revealed an interconnected polymer network with macropores. Within this network, uncalcined MSNs were primarily immobilized in the walls, while some agglomerated clusters were encapsulated in the starch network. The presence of uncalcined MSNs resulted in a rough surface on the MSNs−Cry, which facilitated the adsorption of adsorbates during the adsorption process. After the adsorption experiment, the surface became smoother due to the coverage of MO molecules (Fig. 1c−d) aligning with previous reports [19,32].

The FTIR spectrum of the uncalcined MSNs showed a large absorption band at 3421 cm^{-1} (Fig. 2), assigned to the O–H stretching from silanol (Si–OH) groups, which may interact with defect sites and/or adsorbed water molecules [2,21]. This band overlapped with the O–H stretching from starch molecules, which interacted with Ca^{2+} from the cross−linker [19,23,33,34], resulting in increased intensity in MSNs−Cry. The intensity of this band decreased after MO adsorption, indicating an interaction between the MO structure and OH groups in MSNs−Cry, which likely formed hydrogen bonds with uncalcined MSNs and starch cryogel. Two distinct peaks in uncalcined MSNs at 2922 cm^{-1} and 2852 cm^{-1} corresponded to the C–H stretching of–CH$_3$ and–CH$_2$ groups, respectively, from CTAB molecules embedded inside the nanopores of uncalcined MSNs [2,28,35]. These peaks retained their positions with decreased intensity in MSNs−Cry due to the lower amount of uncalcined MSNs used (2 g) in the composite compared to the starch precursor (80 g). They also retained their positions after MO adsorption. The C–H bending of the alkyl chain in CTAB molecules [36] was also observed at 1480 cm^{-1}, and it retained its position in MSNs−Cry materials. The vibration of O–H bending observed in uncalcined MSNs at 1643 cm^{-1}, which may originate from Si–OH [37] or adsorbed water molecules [25], slightly shifted to 1645 cm^{-1} in MSNs−Cry and to 1648 cm^{-1} after MO adsorption. This confirmed the interaction between the MO structure and OH groups in MSNs−Cry. The intense peak observed at 1063 cm^{-1} in uncalcined MSNs was assigned to asymmetric Si−O−Si stretching [2,21,35], and it retained its position, appearing very close to the vibration of C−O stretching in amylopectin from starch at 1079 cm^{-1} [23,25,38] in MSNs−Cry. Other characteristic vibrations of Si−O−Si [18,28] were also observed in uncalcined MSNs at 1222 cm^{-1} and 793 cm^{-1}. The former seemed to overlap with the vibration from C−O−C asymmetric stretching in glycosidic linkages of starch [25,38,39] at 1156 cm^{-1}, which remained in position after MO adsorption. The vibration of Si−O rocking (452 cm^{-1}) [40] and Si−O stretching of surface Si−OH groups (963 cm^{-1}) [37,40] observed in uncalcined MSNs decreased in intensity in MSNs−Cry, likely due to the lower amount of uncalcined MSNs compared to starch cryogel. The intensities of these peaks were also slightly lower after MO adsorption. New peaks
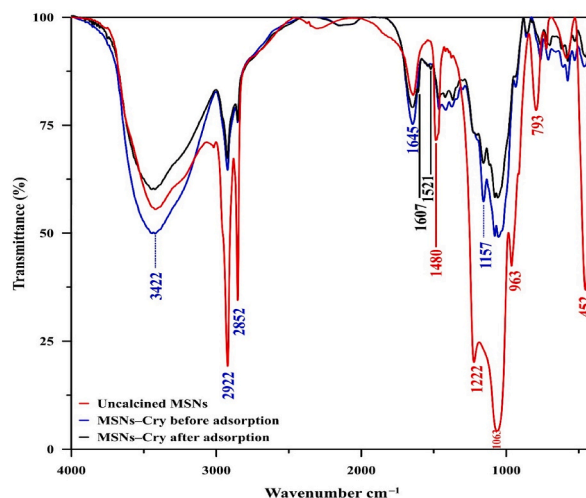

Fig. 2. FTIR spectra of uncalcined MSNs and MSNs−Cry before and after adsorption (KBr pellet sample preparation method, 4000−400 cm^{-1}).

appearing in MSNs−Cry after MO adsorption at 1607 cm^{-1} and 1521 cm^{-1} were corresponded to the −N=N− and −C=C− stretching in aromatic rings [12,41], confirming the adsorption of MO on MSNs−Cry.

The BET analysis of uncalcined MSNs revealed an average pore size of 10.2 nm, a pore volume of 0.04 mL g^{-1}, and a specific surface area of 14 m^2 g^{-1}. The pores of these nanoparticles are larger than those reported for calcined MSNs, which have an average pore size of 2.8 nm, a pore volume of 0.84 mL g^{-1}, and a specific surface area of 1208 m^2 g^{-1} [28]. The difference is due to the CTAB template still embedded inside the nanopores, as confirmed by the FTIR results at 2922 cm^{-1} and 2852 cm^{-1}. For MSNs−Cry, the average pore size was slightly larger at 10.5 nm, with a lower pore volume (0.01 mL g^{-1}) and a specific surface area (3 m^2 g^{-1}). This is due to the immobilization of uncalcined MSNs in the starch cryogel matrix. The pore size distribution of MSNs−Cry showed a wider range compared to the narrower distribution in uncalcined MSNs (Fig. 3a−b). It appears that the uncalcined MSNs were embedded within the starch network, and the starch matrix partially filled the mesopores of the uncalcined MSNs, causing a slight change in the average pore size of MSNs−Cry compared to uncalcined MSNs. Both uncalcined MSNs and MSNs−Cry maintained a type IV adsorption isotherm of N₂ (Fig. 3c−d), indicating their mesoporous nature (micropores <2 nm; mesopores 2−50 nm; macropores >50 nm),
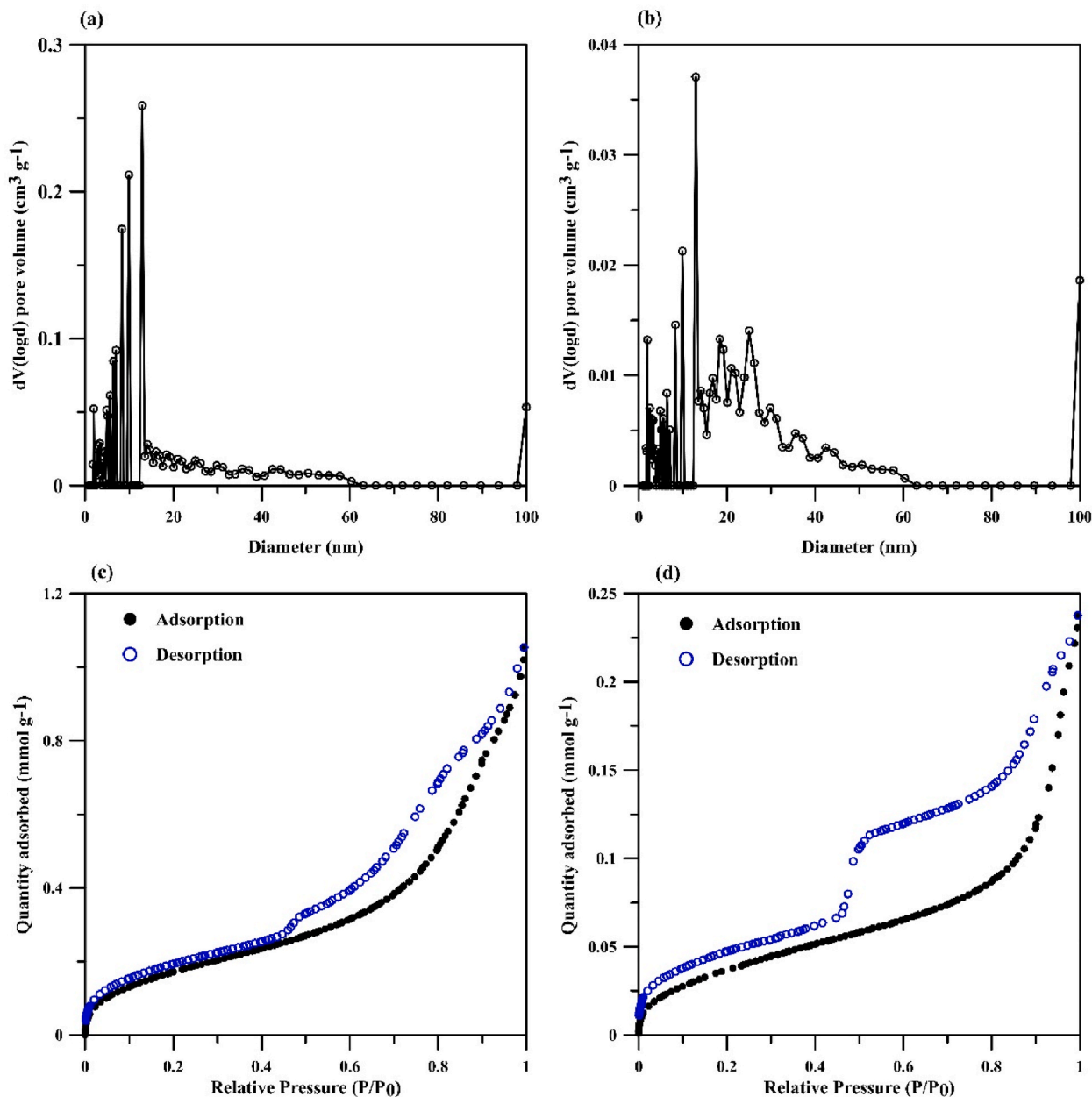

Fig. 3. BET analysis results for (a, c) uncalcined MSNs and (b, d) MSNs−Cry: (a, b) pore size distribution and (c, d) nitrogen adsorption isotherm (degassed at 105 °C for 30 min before analyzing the nitrogen adsorption/desorption isotherm at 77 K).

consistent with previous reports [27,28,42]. However, the hysteresis loop of MSNs−Cry differed from that of uncalcined MSNs, indicating changes in pore sizes and shapes due to the immobilization of uncalcined MSNs within the starch network. The H3 hysteresis loop observed in uncalcined MSNs suggested slit−shaped pores in non−rigid aggregates of plate−like particles [28,43], while the H2 hysteresis loop observed in MSNs−Cry indicated a variety of pore types with a larger distribution of pore diameters, including neck−like, wide, or ink bottle−shaped pores [43].

The XRD pattern of uncalcined MSNs displays a peak at 2θ ~4.39° (Supplementary Materials Fig. S1), which is attributed to the (200) plane of a less ordered hexagonal structure of silica nanoparticles [44]. This suggests that uncalcined MSNs may contain nanoparticles with a certain degree of structural ordering, as this peak has been reported to appear when MSNs are prepared with excess CTAB [28,45]. Additionally, a broad peak at 2θ ~20.1°, corresponding to amorphous silica nanoparticles with (101) planes [12, 46,47], was also observed. These indicated that both a less ordered hexagonal structure and amorphous silica nanoparticles are present in uncalcined MSNs. However, when uncalcined MSNs are embedded within the starch cryogel matrix, the peak at 2θ ~4.39° disappears, indicating a loss of nanoparticle order. The broad peak from amorphous silica nanoparticles in uncalcined MSNs may overlap with a broad hump centered at 2θ ~20°, due to the amorphous structure of starch [23,25] in MSNs−Cry. Sharp peaks at 2θ ~12.9°, 14.8°, 17.0°, and 19.9° indicate an A−type crystalline structure of rice starch [23,25], suggesting that some crystallinity of the starch granule remains. This crystallinity is typically disrupted during gelatinization and cross−linking with Ca^{2+} [23,25]. After MO adsorption, MSNs−Cry showed the same XRD pattern, indicating the retention of their amorphous structure.

The EDX analysis of uncalcined MSNs reveals the presence of Si and O (Table 1 and Supplementary Materials Fig. S2). These elements are also found in MSNs−Cry, as the uncalcined MSNs were embedded within the starch cryogel network. Ca was detected in MSNs−Cry due to the use of limewater as the cross−linker. After MO adsorption, the presence of S confirmed the adsorption of MO on MSNs−Cry.

The zeta potential of both uncalcined MSNs and MSNs−Cry was investigated. The results showed that the zeta potential of uncalcined MSNs at pH 7.59 was $+21.12 \pm 0.87$ mV, in contrast to calcined MSNs reported in the literature (e.g., -29.7 mV at pH 7.4 [48], -42 mV [49]). This indicates a positively charged surface, likely due to the presence of CTAB in the material. When uncalcined MSNs were incorporated into the starch cryogel matrix to produce MSNs−Cry, the zeta potential decreased to $+4.48 \pm 0.32$ mV but remained positive. This confirms that MSNs−Cry retains a positively charged surface, which is expected to facilitate the adsorption of MO through electrostatic attraction between its positive surface and the anionic dye.

The DSC thermograms of uncalcined MSNs and MSNs−Cry are reported in Supplementary Materials, Fig. S3. All materials exhibited multiple endothermic peaks, indicating the presence of various polymorphic forms in the materials. A broad endothermic peak was observed in all materials within the range of 50–120 °C (peak temperature = 75.17 °C for uncalcined MSNs and 77.17 °C for MSNs−Cry), which can be attributed to moisture desorption [50,51]. In MSNs−Cry, this peak may also be related to the gelatinization of calcium-crosslinked starch, previously reported at a peak temperature of 78 °C [52], resulting in a higher peak area compared to uncalcined MSNs. The peak observed in the range of 160–280 °C in uncalcined MSNs (peak temperature = 226.50 °C) may be attributed to the decomposition of CTAB, similar to previously reported findings [46], as the melting point of CTAB is 248–251 °C. The smaller area of this peak in MSNs−Cry indicates a lower CTAB content compared to uncalcined MSNs, which is expected due to the 2.5 % w/w of uncalcined MSNs present in MSNs−Cry. Additionally, this peak disappeared in MSNs−Cry after MO adsorption, which may suggest that CTAB strongly interacts with MO, resulting in no loss during the analysis. The multiple peaks in MSNs−Cry, within the range of 270–341 °C, may be attributed to the elimination of hydroxyl groups and the decomposition and depolymerization of carbon chains [53]. Additionally, it was found that the first and last peaks in this region disappeared from MSNs−Cry after MO adsorption, suggesting that MO may strongly interact with the hydroxyl groups in the starch cryogel, resulting in a more stable form of the material. This stability prevents the loss or decomposition and depolymerization of carbon chains during the analysis. An exothermic peak was also observed in MSNs−Cry after MO adsorption, between 279 and 315 °C (peak temperature = 304.5 °C), corresponding to the melting of MO crystals adsorbed on MSNs−Cry, as the melting point of MO is reported to be around 300 °C.

3.2. Methyl orange adsorption

Appropriate conditions for MO adsorption were systematically optimized by varying one parameter at a time while keeping others constant. The initial conditions are described in Section 2.2. This approach not only provided the optimal conditions but also demonstrated the influence of each parameter on the removal efficiency and capacity of MO using MSNs−Cry.

Table 1
Elemental analysis of uncalcined MSNs and MSNs−Cry before and after adsorption experiment analyzed by energy dispersive X−ray spectroscopy (EDX).

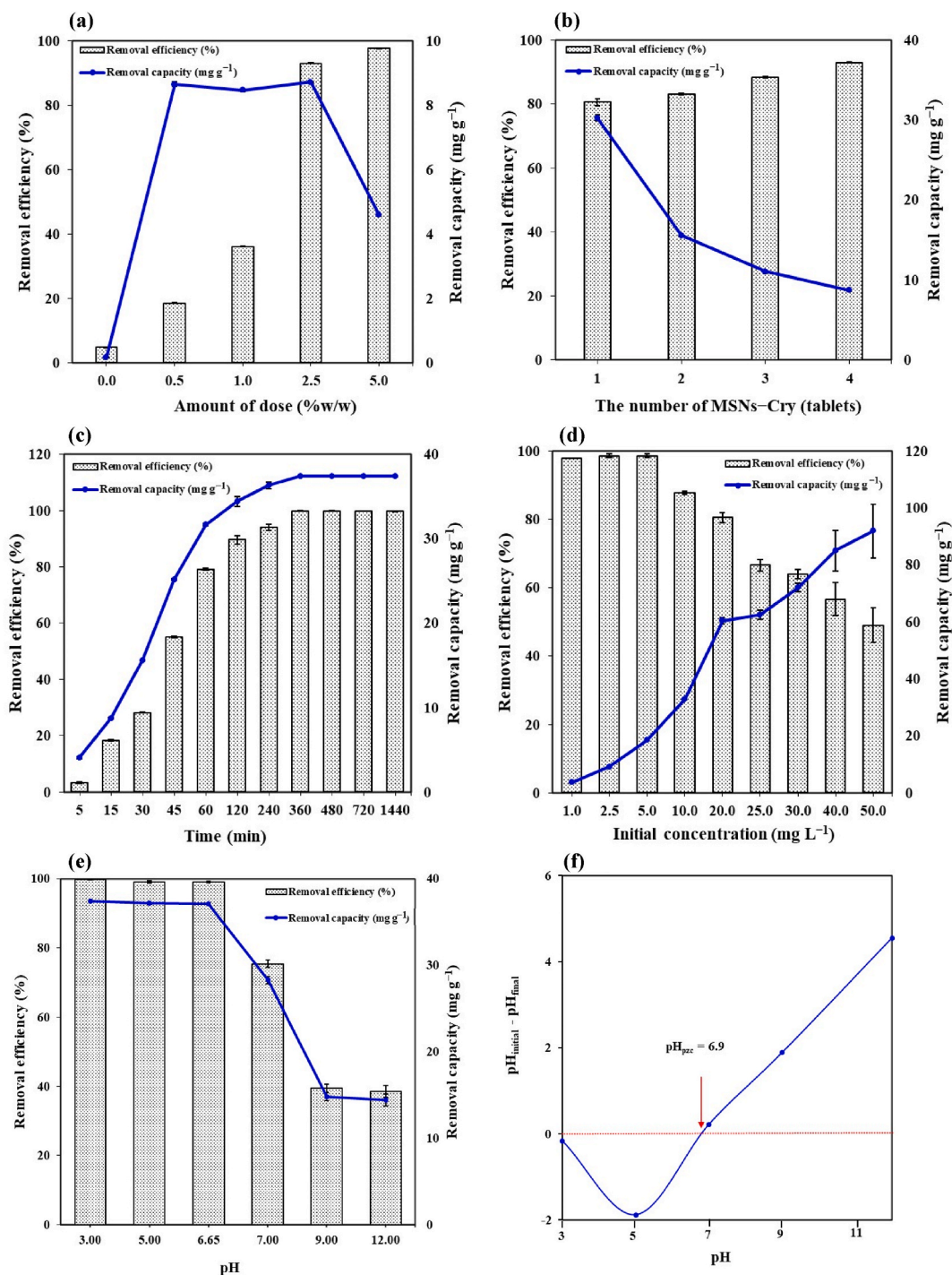| Elements	Uncalcined MSNs (%*wt*)	MSNs−Cry (%*wt*)	
		Before adsorption	After adsorption
C	42.4 ± 0.2	49.0 ± 0.2	50.5 ± 0.2
O	36.6 ± 0.2	47.8 ± 0.2	46.6 ± 0.2
Si	21.0 ± 0.1	2.8 ± 0.0	2.5 ± 0.0
Ca		0.4 ± 0.0	0.2 ± 0.0
S			0.3 ± 0.0

Fig. 4. Influence of (a) the amount of uncalcined MSNs in MSNs−Cry (Adsorption conditions: 0.35 g MSNs−Cry, 10 mg L^{-1} MO, 300 mL, pH 6.65, 25 °C; 2 h contact time), (b) the number of MSNs−Cry tablets (Adsorption conditions: 10 mg L^{-1} MO, 300 mL, pH 6.65, 25 °C; 2 h contact time), (c) contact time (Adsorption conditions: 0.35 g MSNs−Cry, 10 mg L^{-1} MO, 300 mL, pH 6.65, 25 °C), (d) initial MO concentration (Adsorption conditions: 0.35 g MSNs−Cry, 300 mL MO, pH 6.65, 25 °C; 2 h contact time), and (e) initial solution pH on the removal efficiency and capacity of MO by MSNs−Cry (Adsorption conditions: 0.35 g MSNs−Cry, 10 mg L^{-1} MO, 300 mL, 25 °C; 2 h contact time). (f) Point of zero charge of MSNs−Cry (Conditions described in Supplementary Materials S4).

3.2.1. Influence of adsorbent dosage

The optimal amount of uncalcined MSNs in MSNs−Cry for achieving high removal efficiency of MO with reasonable adsorption capacity was investigated by varying the dosage of uncalcined MSNs from 0 to 4 g in 80 g of a starch gel precursor (0–5 % w/w). The results (Fig. 4a) showed that as the amount of uncalcined MSNs in MSNs−Cry increased, the removal efficiency rose from 4.72 % $\pm$ 0.14 %–97.67 % $\pm$ 0.08 %. However, the adsorption capacity decreased from 8.64 $\pm$ 0.06 mg g^{-1} to 4.58 $\pm$ 0.03 mg g^{-1}. The highest adsorption capacity, 8.71 $\pm$ 0.01 mg g^{-1}, was achieved with MSNs−Cry prepared using 2 g of uncalcined MSNs (2.5 % w/w), which also had a high removal efficiency of 92.92 % $\pm$ 0.14 %. This efficiency was only 4.56 % lower than the highest removal efficiency of 97.67 % $\pm$ 0.08 %, which was achieved with 4 g of uncalcined MSNs (5 % w/w). Therefore, 2 g of uncalcined MSNs (2.5 % w/w) was chosen for preparing MSNs−Cry. It is noteworthy that the starch cryogel without uncalcined MSNs could remove MO with a removal efficiency of 4.72 % $\pm$ 0.14 % due to the available OH groups in its structure.

The resulting MSNs−Cry monolithic rod, prepared from 2.5 % w/w of uncalcined MSNs in a starch gel precursor, was divided into 4 pieces to form MSNs−Cry tablets. The number of tablets was then varied from 1 to 4 (0.35 g each). The results (Fig. 4b) showed that as the number of MSNs−Cry tablets increased, the removal efficiency improved from 79.16 % $\pm$ 0.34 %–92.92 % $\pm$ 0.14 %, while the adsorption capacity decreased from 29.68 $\pm$ 0.13 mg g^{-1} to 8.71 $\pm$ 0.01 mg g^{-1}. Therefore, one MSNs−Cry tablet was selected for further investigation. However, for real samples with high concentrations of MO, additional tablets can be used to increase removal efficiency.

3.2.2. Influence of contact time

The effect of contact time on the adsorption efficiency of MO on MSNs−Cry was investigated using one piece of MSNs−Cry (0.35 g). The removal efficiency of MO increased gradually, reaching 87.75 % $\pm$ 0.55 % within 120 min, then slightly increased to 99.78 % $\pm$ 0.14 % at 360 min, and finally plateaued (Fig. 4c). The adsorption capacity followed a similar pattern: an initial gradual increase, followed by a slight rise, and then a constant level. This behavior can be attributed to the availability of unoccupied surface sites, which are more abundant at the beginning of contact, decrease in the second stage, and become fully occupied by the end of the process, leading to constant removal efficiency and capacity [18]. The results showed that the adsorption of MO on MSNs−Cry reached equilibrium after 6 h. This is faster than the 24 h required when using CTAB−coated porous silica nanoparticles [54], but longer than the 20 min needed for MCM−41 to reach equilibrium [18]. Although MSNs−Cry contain macropores that help MO reach the active sites, the cryogel matrix can slow down the penetration of MO to the MSNs compared to MCM−41 nanoparticles, resulting in a longer equilibrium time.

3.2.3. Influence of initial concentration

The effect of initial concentration was studied from 1.0 to 50.0 mg L^{-1}. The results presented that the removal efficiency of MO (97.80 % $\pm$ 0.00 %–98.56 % $\pm$ 0.57 %) remained nearly constant as the initial concentration increased from 1.0 to 5.0 mg L^{-1}, then tended to decrease with higher concentrations (Fig. 4d). At low concentrations, the ratio of MO to available active sites on MSNs−Cry is low, resulting in high removal efficiency. As the initial MO concentration increases, this ratio rises, leading to some MO not occupying the limited active sites on MSNs−Cry, thereby decreasing the removal efficiency [21,55]. Conversely, the adsorption capacity rose with the initial MO concentration, reaching a maximum of 91.88 $\pm$ 9.42 mg g^{-1} at 50 mg L^{-1}. The increase in initial MO concentration resulted in a higher mass gradient of MO between the solution and the active sites of MSNs−Cry. This gradient creates a driving force that enhances the transport of MO molecules from the bulk solution to the binding sites, leading to an increase in adsorption capacity [29,56].

3.2.4. Influence of pH

The effect of initial pH on the adsorption of MO onto MSNs−Cry was investigated over a pH range of 3–12. The results, shown in Fig. 4e, indicate higher adsorption capacity and efficiency under acidic conditions. This is likely due to the point of zero charge (pH$_{pzc}$, as detailed in Supplementary Material S4) of MSNs−Cry, found to be at pH 6.9 (Fig. 4f). Below this pH, the surface of MSNs−Cry is positively charged, while above it, the surface is negatively charged. Therefore, greater adsorption of MO is expected in acidic conditions, where electrostatic attraction occurs between the anionic MO (pK$_a$ = 3.4 [3]) and the positively charged surface of MSNs−Cry. These findings are consistent with previous reports. For example, CTAB−modified coffee waste achieved the highest adsorption at pH 3.5 [57], and uncalcined MCM−48 showed the highest adsorption of MO at pH 3.0 [2]. The lower adsorption capacity and efficiency at higher pH levels can be attributed to electrostatic repulsion between the negatively charged surface of MSNs−Cry and the negatively charged MO molecules, as well as competition from OH$^-$ ions and dye anions for adsorption sites [2,58−60]. Since a removal efficiency of 99.00 % $\pm$ 0.21 % was achieved at pH ~6.65, which is close to the typical pH of wastewater from the batik industry (~6.91), it is not necessary to adjust the pH of real samples, eliminating a potential cost in real−world applications.

3.3. Adsorption isotherms, kinetics, and thermodynamics

The adsorption capacity of MSNs−Cry was determined at different initial MO concentrations to understand the adsorption behavior of MO on MSNs−Cry. Both the Langmuir and Freundlich models were used to describe the relationship between the amount of MO adsorbed by MSNs−Cry and its equilibrium concentration in the aqueous solution. The Langmuir model provided a better fit (R^2 = 0.9930) (Supplementary Materials Fig. S4a) than the Freundlich model (R^2 = 0.9180) (Supplementary Materials Fig. S4b). According to the Langmuir model, the Q$_{max}$ was estimated to be 18.98 mg g^{-1}, with a constant (k$_L$) of 0.977 L mg^{-1} (Table 2). When considering only the weight of MSNs, the Q$_{max}$ increased to 72.46 mg g^{-1}, with a k$_L$ of 0.783 L mg^{-1}. The dimensionless constant R$_L$ value decreased

from 0.50 to 0.02 as the initial MO concentration rose from 1 to 50 mg L^{-1}, indicating more favorable adsorption at higher concentrations [61,62]. These results suggest that MO is likely adsorbed onto MSNs−Cry as a monolayer at specific homogeneous sites within MSNs−Cry.

The adsorption kinetic study is crucial for understanding the adsorption mechanism and its rate. The experimental results were fitted to both pseudo−first−order (PFO) and pseudo−second−order (PSO) kinetic models, with the calculated kinetic parameters provided in Table 2. The PSO model yielded a better fit, with a higher R^2 value of 0.9917 (Supplementary Materials Fig. S4c−d). Additionally, the estimated Q_e from the PSO model (9.09 mg g^{-1}) approached the experimental Q_e (8.56 mg g^{-1}). When considering only the weight of MSNs, the estimated Q_e from the PSO model was 38.46 mg g^{-1}, which was also close to the experimental Q_e (37.44 mg g^{-1}). This suggests that the PSO model more accurately describes the MO adsorption process, aligning with previous studies on silica materials [2,18,57]. The results demonstrated that the adsorption of MO on MSNs−Cry involves multiple mechanisms, including electrostatic attraction and other chemical interactions. The k_2 value of 0.002 g mg^{-1} min^{-1} was higher than the reported value for MCM−48 (0.001 g mg^{-1} min^{-1}) [2]. However, with uncalcined MSNs entrapped within the cryogel matrix, the smooth approach of MO to the active sites might have been disrupted [19,22]. The higher k_2 value could be attributed to the presence of macropores in MSNs−Cry, which likely aided MO in reaching the active sites more easily. Nonetheless, it remained lower than that observed for MCM−41 particles (0.006 g mg^{-1} min^{-1}) [18].

The intra−particle diffusion model was also analyzed to describe the diffusion mechanism and determine the rate−determining step. The plot using this model (Supplementary Materials Fig. S5) did not intersect the origin and was segmented into three sections with different slopes, indicating three stages of MO adsorption on MSNs−Cry with varying rates. Initially, MO molecules permeated the outer surface of MSNs−Cry through film diffusion at a faster rate. This was followed by diffusion into the internal pores of MSNs−Cry through intraparticle diffusion at a slower but more stable pace, suggesting that this step determined the overall rate. Finally, equilibrium was reached. These results indicate that MO is adsorbed onto both the surface and internal structure of MSNs−Cry.

The adsorption thermodynamics were also investigated to understand the nature and energetic changes involved during MO adsorption. The changes in standard Gibbs free energy ($\Delta G°$), enthalpy ($\Delta H°$), and entropy ($\Delta S°$) for MO adsorption on MSNs−Cry are presented in Supplementary Materials Table S3, with the plots shown in Supplementary Materials Fig. S6. The negative $\Delta G°$ values at all temperatures ($\Delta G° = -34.2$ to -38.6 kJ mol^{-1}) indicate that the adsorption of MO on MSNs−Cry is spontaneous, with more favorable adsorption observed at higher temperatures. It is reported that the absolute magnitude of $\Delta G°$ for physisorption generally ranges from -20 to 0 kJ mol^{-1}, while for chemisorption it ranges from -80 to -400 kJ mol^{-1} [63,64]. The obtained results fell between these two ranges, indicating a form of physical adsorption that is enhanced by a chemical effect. The positive $\Delta H°$ ($\Delta H° = 31.3$ kJ mol^{-1}) indicates that MO adsorption is endothermic, while the positive $\Delta S°$ values ($\Delta S° = 219.7$ J mol^{-1} K^{-1}) indicate an increase in degree of disorder at the solid−solution interface during the adsorption process.

3.4. Influence of interferences

The effect of potential interferences in batik wastewater [65,66], including sodium silicate, sodium sulfate, urea, heavy metal ions (K^+, Pb^{2+}, Cu^{2+}, Cd^{2+}, and Zn^{2+}), and the anionic dye Congo Red (CR), was investigated. These potential interferences were mixed with MO before the adsorption process using MSNs−Cry under optimum conditions. The results revealed that the removal efficiency of MO remained above 92 % in the presence of metal ions (Table 3), indicating that metal ions commonly present in batik wastewater had no effect on the removal process. In the presence of CR, the removal efficiency of MO remained consistent at 93.51 % ± 1.31 %. Additionally, CR was efficiently removed by MSNs−Cry at a rate of 91.77 % ± 0.40 % when MO was present and 92.93 % ± 0.18 % when MO was absent. This demonstrates the excellent performance of MSNs−Cry for the simultaneous removal of anionic dyes. Since CR is a diazo dye with similar functional groups (two sulfonic and azo groups with aromatic rings) to those of MO (one sulfonic and azo group with aromatic rings), the similar removal performance of both dyes confirms the proposed removal mechanism, which is expected to be based on electrostatic attraction, hydrophobic interaction, and hydrogen bonding. Additionally, since CR has a larger molecular size than MO but does not exhibit a steric hindrance effect on the adsorption efficiency of CR compared to MO, the pore filling of these dyes

Table 2
The estimated isotherm and kinetic parameters for adsorption of MO onto MSNs−Cry.

Model	Parameter	Value
Langmuir	k_L (L mg^{-1})	0.977
	Q_{max} (mg g^{-1})	18.98
	R^2	0.9930
Freundlich	K_F (mg^{1-n} L^n g^{-1})	6.69
	$1/n$	0.38
	R^2	0.9180
Pseudo−first−order	Q_e, experiment (mg g^{-1})	8.56
	k_1 (g mg^{-1} min^{-1})	0.002
	Q_e, estimated (mg g^{-1})	5.80
	R^2	0.9685
Pseudo−second−order	Q_e, experiment (mg g^{-1})	8.56
	k_2 (g mg^{-1} min^{-1})	0.002
	Q_e, estimated (mg g^{-1})	9.09
	R^2	0.9917

onto MSNs−Cry should not occur as it does with other silica materials [47]. The simultaneous removal of MO and CR under the same conditions highlights the potential of MSNs−Cry for real−world applications where wastewater may contain multiple dyes simultaneously. However, the removal efficiency decreased to 84.88 % ± 1.14 % in the presence of urea and sodium sulfate, and further decreased to 59.68 % ± 3.11 % in the presence of sodium silicate. This reduced efficiency may be attributed to the interaction between the smaller, negatively charged silicate moiety and the positively charged surface of MSNs−Cry.

3.5. Proposed mechanism

Due to the use of uncalcined MSNs in MSNs−Cry, the cationic template (CTAB) remains within its structure, along with the complex structure of MO. Consequently, multiple interactions between anionic MO and MSNs−Cry are expected. The results from FTIR analysis and the influence of pH suggest that the primary interaction between MO and MSNs−Cry is based on the electrostatic attraction between the sulfonic acid groups ($-SO_3^-$) in the MO structure and the positive heads of CTAB ($R-N^+(CH_3)_3$) present in MSNs−Cry [2, 12,47,67]. Additionally, the peak at 226.50 °C in the DSC thermogram of MSNs−Cry, attributed to the decomposition of CTAB [46], disappeared after MO adsorption, suggesting that CTAB strongly interacts with MO, preventing any loss during the analysis. The results from the zeta potential analysis, showing a decrease in the positive surface charge of uncalcined MSNs from $+21.12 \pm 0.87$ mV to $+14.14 \pm 0.83$ mV after MO adsorption, further confirm that MO interacts with the CTAB moiety, leading to the adsorption of MO on the material. Additionally, since the adsorption occurred at pH 6.65, some of the silanol groups from uncalcined MSNs and OH groups on the cryogel surface may become protonated to form OH_2^+, thereby participating in this attraction [2,60]. Available OH groups in MSNs−Cry, originating from both the silanol groups in uncalcined MSNs and the OH groups on the cryogel surface, can also form hydrogen bonds with the sulfonyl group and azo group in MO molecules [2,47,60,68]. The DSC analysis of MSNs−Cry after MO adsorption shows that the first and last peaks in the range of 270–341 °C, which are attributed to the elimination of hydroxyl groups and the decomposition and depolymerization of carbon chains [53], have disappeared. This observation confirms the strong interaction between MO and the hydroxyl groups in MSNs−Cry, resulting in a more stable material that prevents the loss, decomposition, or depolymerization of carbon chains during the analysis. Furthermore, the atomic cycles in the MO molecule may interact with the alkyl part of CTAB in MSNs−Cry via hydrophobic–hydrophobic interactions [2,12,67,69]. Both electrostatic interaction and hydrogen bonding related to the OH groups on the cryogel surface account for the 4.72 % ± 0.14 % removal efficiency obtained from the material without uncalcined MSNs. The incorporation of uncalcined MSNs into starch cryogel enhanced the removal efficiency of MO to 92.92 % ± 0.14 %. This suggests that electrostatic interactions, hydrogen bonding, and hydrophobic–hydrophobic interactions from uncalcined MSNs in MSNs−Cry account for approximately 88.2 % of the removal efficiency, compared to about 4.7 % from the starch cryogel. This confirms that uncalcined MSNs act as the primary active material for MO removal, while the starch cryogel, serving as a supporting material, synergistically enhances the removal efficiency by approximately 5 %. The proposed mechanism is illustrated in Fig. 5.

Using uncalcined MSNs makes the MSNs−Cry greener than other reported MSNs materials, as it eliminates the need for calcination, conserving energy and aligning with green chemistry principles. Additionally, using starch cryogel as a green support helps prevent the loss and aggregation of uncalcined MSN particles, making the developed material suitable for future continuous flow systems.

3.6. Real sample application

MSNs−Cry was used to remove MO from three wastewater samples collected from a local batik industry in Phuket, Thailand (experimental conditions are described in Supplementary Material S5). As shown in Fig. 6, the UV–visible spectrum and appearance of the real sample changed after 2 h of adsorption using MSNs−Cry. The color of the sample changed from dark to colorless, while the concentration of MO decreased to less than 0.48 ± 0.06 mg L^{-1} (Table 4), achieving a high removal efficiency of 86.34 % ± 1.65 %–92.77 % ± 1.76 %. After treatment, the pH of sample A slightly increased from 6.86 to 7.20. The chemical oxygen demand (COD) rose from 9.8 to 39.1 mg L^{-1}, while total suspended solids (TSS) decreased from 24.67 to 2.67 mg L^{-1}. These values are within the maximum discharge guidelines for municipal wastewater treatment plants in Thailand (pH 6−9, COD ≤120 mg L^{-1}, TSS ≤50 mg L^{-1}) [70]. All samples were spiked with 15 mg L^{-1} of MO before applying MSNs−Cry under the same experimental conditions to assess the effect of the sample matrix. A removal efficiency of 80.08 % ± 0.47 %–85.12 % ± 0.36 % was achieved, demonstrating the strong performance of MSNs−Cry for MO removal, even in high-concentration samples. As the spiked samples contained more MO than the

Table 3
Removal efficiency and capacity of MO in the presence of various interferences using MSNs−Cry.

Interference	RE (%)	%Change in RE
None (MO, 10 mg L^{-1})	92.92 ± 0.14	–
CR[a]	93.51 ± 1.31	+0.63
metal ions[b]	92.87 ± 0.23	−0.05
urea + sodium sulfate[c]	84.88 ± 1.14	−8.65
sodium silicate[d]	59.68 ± 3.11	−35.77

[a] 10 mg L^{-1} of congo red.
[b] 1 mg L^{-1} of Cu^{2+}, Pb^{2+}, Zn^{2+}, K^+, and Cd^{2+}.
[c] 1000 mg L^{-1} of urea and sodium sulfate; and.
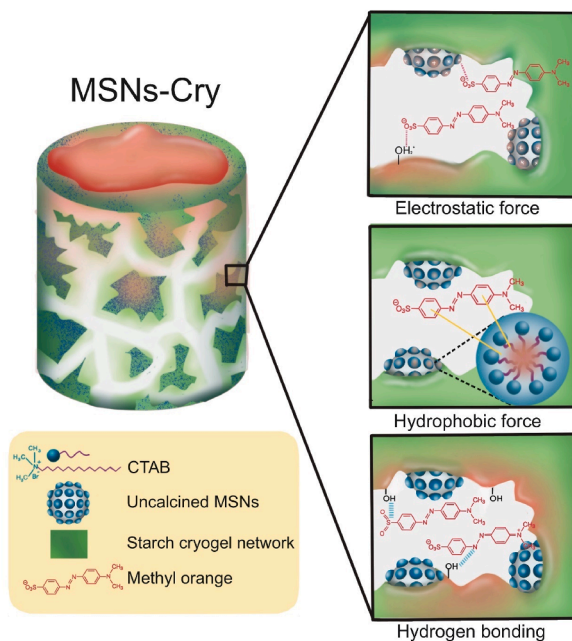[d] 137 mg L^{-1} of sodium silicate.

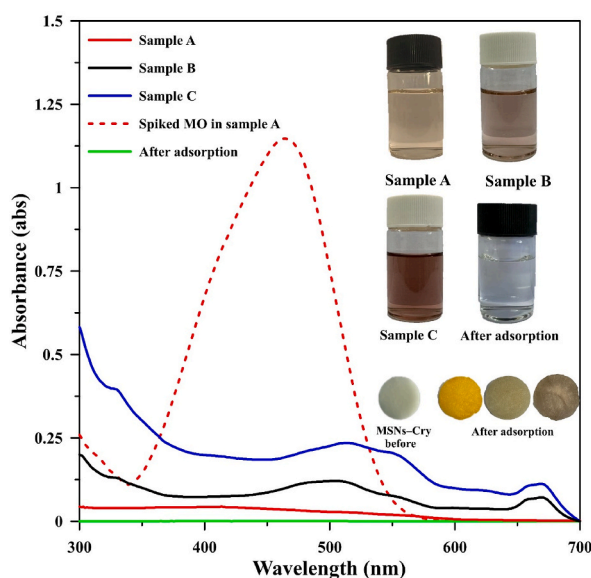**Fig. 5.** The proposed mechanism for adsorption of MO on MSNs−Cry.

Fig. 6. UV–visible spectrum and appearance of the real samples and MSNs−Cry before and after adsorption.

synthetic wastewater (10 mg L^{-1} MO), a higher dose of MSNs−Cry was required. The removal efficiency was then evaluated using 0.70 g of MSNs−Cry, compared to 0.35 g in real samples without spiked MO. The results showed excellent removal efficiency (91.56 % ± 0.66 %–92.57 % ± 0.99 %), highlighting the strong potential of MSNs−Cry for MO removal in real-world applications.

3.7. Reusability

The reusability of MSNs−Cry was evaluated using 0.1 M NaOH as the desorbing reagent [30,60]. The removal efficiency of MO decreased by 36.25 % in the second cycle. This decrease may be attributed to the dissolution of CTAB remaining in MSNs−Cry in the NaOH solution, resulting in less CTAB available for the next cycle. Additionally, during the second regeneration process, the tablets were damaged into smaller fragments. This may be because starch cryogel was used as the natural support instead of other synthetic polymers, and its swelling in the aqueous solution led to lower tolerance under continuous stirring conditions.

Table 4
Application of MSNs−Cry for the removal of MO in real wastewater samples.

Sample	Concentration of MO (mg L^{-1})		%RE
	Before	After	
Sample A[a]	0.43 ± 0.02	0.03 ± 0.01	92.77 ± 1.76
Sample B[a]	1.90 ± 0.02	0.22 ± 0.03	88.24 ± 1.74
Sample C[a]	3.54 ± 0.02	0.48 ± 0.06	86.34 ± 1.65
Spiked sample A[a]	15.21 ± 0.03	2.26 ± 0.06	85.12 ± 0.36
Spiked sample B[a]	16.93 ± 0.10	3.29 ± 0.20	80.56 ± 1.12
Spiked sample C[a]	18.81 ± 0.20	3.75 ± 0.12	80.08 ± 0.47
Spiked sample A[b]	15.43 ± 0.01	1.15 ± 0.15	92.57 ± 0.99
Spiked sample B[b]	15.83 ± 0.01	1.19 ± 0.08	92.47 ± 0.48
Spiked sample C[b]	18.47 ± 0.04	1.56 ± 0.12	91.56 ± 0.66

[a] Conditions: 0.35 g of MSNs−Cry, 300 mL wastewater samples, without adjusting the pH (pH ∼ 6.86), 25 °C, 2 h.
[b] Conditions: 0.70 g of MSNs−Cry, 300 mL wastewater samples, without adjusting the pH (pH ∼ 6.86), 25 °C, 2 h.

From the results, it's clear that MSNs−Cry could be an effective alternative adsorbent for removing MO. Table 5 compares MSNs−Cry with various materials for MO removal, highlighting its high efficiency and capacity. Moreover, it prevents the loss of uncalcined MSNs during adsorption, which could negatively impact both the operation system and the environment. The entrapment of uncalcined MSNs within the starch cryogel matrix led to a milder pH condition. MSNs−Cry showed excellent removal efficiency at a pH 6.65 without needing adjustment. This not only allows for operation under gentler conditions but also saves on the costs associated with pH adjustment. Additionally, using uncalcined MSNs instead of modified calcined mesoporous silica materials (e.g., MCM−41, MCM−48) can save energy and reduce material preparation costs.

4. Conclusion

In conclusion, this study introduced a novel, eco−friendly composite, MSNs−Cry, which effectively embeds uncalcined MSNs within a starch cryogel network for the removal of MO from water. The proposed adsorption mechanism primarily involves electrostatic attraction, hydrophobic interactions, and hydrogen bonding. MO adsorption onto MSNs−Cry occurs as a monolayer at specific homogeneous sites on both the surface and internal structure of the composite. The adsorption process is characterized as endothermic, spontaneous, and more favorable at higher temperatures. The composite leverages the high adsorption capacity of MSNs, achieving a maximum adsorption capacity of 18.98 mg g^{-1} and high removal efficiency of 99.00 % ± 0.21 % in synthetic water, as well as 92.77 % ± 1.76 % in real wastewater. Its high efficiency remained even in the presence of potential interferences in batik wastewater, including metal ions and other anionic dyes. However, some negative effects were observed from sodium silicate, which, due to its smaller size and negative charge, could compete with MO for adsorption. Additionally, the tablet form of MSNs−Cry prevents the loss of uncalcined MSNs during adsorption, mitigating potential negative impacts on both the operational system and the environment. Furthermore, its ability to operate effectively at milder pH conditions without the need for pH adjustment offers a cost−saving advantage for real−world applications. This study demonstrates that MSNs−Cry is a promising material for efficient and sustainable water purification.

CRediT authorship contribution statement

Tarawee Taweekarn: Writing – original draft, Visualization, Validation, Methodology, Investigation, Data curation, Conceptualization. **Worawit Wongniramaikul:** Writing – review & editing, Validation, Resources, Methodology, Funding acquisition, Data curation, Conceptualization. **Wilasinee Sriprom:** Writing – review & editing, Data curation. **Wadcharawadee Limsakul:** Data curation. **Chanadda Phawachalotorn:** Writing – review & editing, Validation, Data curation. **Aree Choodum:** Writing – review & editing, Writing – original draft, Validation, Supervision, Resources, Project administration, Methodology, Funding acquisition, Data curation, Conceptualization.

Data availability statement

All data are available from the corresponding author on reasonable request.

Funding

Declaration of competing interest

The authors declare that they have no known competing financial interests or personal relationships that could have appeared to

Table 5
Adsorption parameters for the removal of MO using various materials.

Material	Form	Q_{max} (mg $g_{active\ material}^{-1}$)	pH	Contact time (min)	Reference
Populous leaves	Particle	90.44	3.0	60	[59]
Co_3O_4 nanoparticle	Particle	46.08	6.0	240	[71]
Cork powder	Particle	16.66	2.0	240	[72]
Chitosan/diatomite composite	Particle	35.12	5.0	40	[30]
Fe$-$MCM$-$41	Particle	500	2.0	10	[18]
MCM$-$48	Particle	769.23	3.0	30	[2]
Fe_3O_4@SiO_2	Particle	182.503	2.0	30	[60]
Calcined MSNs	Particle	69.40	4.0	240	[47]
MSNs$-$Cry	Tablet	72.46	6.65	120	This work

influence the work reported in this paper.

Acknowledgment

Appendix A. Supplementary data

Supplementary data to this article can be found online at https://doi.org/10.1016/j.heliyon.2024.e39711.

References

[1] S. Allen, B. Koumanova, *Decolourisation of water/wastewater using adsorption.* Journal of the university of chemical technology and metallurgy 40 (3) (2005) 175–192.
[2] M. Anbia, S. Salehi, Adsorption of methyl-orange from aqueous solution onto nanoporous silica materials, Sci. Iran. 21 (2014) 2036–2048.
[3] K.O. Iwuozor, et al., Adsorption of methyl orange: a review on adsorbent performance. Current Research in Green and Sustainable Chemistry 4 (2021) 100179.
[4] P.K. Malik, Dye removal from wastewater using activated carbon developed from sawdust: adsorption equilibrium and kinetics, J. Hazard Mater. 113 (1–3) (2004) 81–88.
[5] S.A. Mousavi, et al., Methylene blue removal using grape leaves waste: optimization and modeling, Appl. Water Sci. 12 (5) (2022) 112.
[6] V.K. Garg, et al., Dye removal from aqueous solution by adsorption on treated sawdust, Bioresour. Technol. 89 (2) (2003) 121–124.
[7] F. Nekouei, et al., *Kinetic, thermodynamic and isotherm studies for acid blue 129 removal from liquids using copper oxide nanoparticle-modified activated carbon as a novel adsorbent.* Journal of Molecular Liquids 201 (2015) 124–133.
[8] J. Paul Guin, Y.K. Bhardwaj, L. Varshney, Mineralization and biodegradability enhancement of Methyl Orange dye by an effective advanced oxidation process, Appl. Radiat. Isot. 122 (2017) 153–157.
[9] B. Jiang, et al., Degradation of azo dye using non-thermal plasma advanced oxidation process in a circulatory airtight reactor system, Chem. Eng. J. (2012) 32–39, 204-206.
[10] M.M. Islam, S. Basu, Effect of morphology and pH on (photo)electrochemical degradation of methyl orange using TiO2/Ti mesh photocathode under visible light. Journal of Environmental Chemical Engineering 3 (4, Part A) (2015) 2323–2330.
[11] S.-H. Li, et al., Electrochemical degradation of methyl orange on Pt–Bi/C nanostructured electrode by a square-wave potential method, Electrochim. Acta 92 (2013) 93–101.
[12] F. Sadegh, et al., *Magnetically recyclable Fe3O4–CuS@SiO2 catalyst for synergistic adsorption and photodegradation of methyl orange in wastewater under visible light.* Environmental Technology & Innovation 33 (2024) 103545.
[13] M. Adeel, et al., Synthesis and characterization of Co-ZnO and evaluation of its photocatalytic activity for photodegradation of methyl orange, ACS Omega 6 (2) (2021) 1426–1435.
[14] J. Luo, et al., Enhanced photodegradation activity of methyl orange over Ag2CrO4/SnS2 composites under visible light irradiation, Mater. Res. Bull. 77 (2016) 291–299.
[15] Z.-x. Chen, et al., Removal of methyl orange from aqueous solution using bentonite-supported nanoscale zero-valent iron. Journal of Colloid and Interface Science 363 (2) (2011) 601–607.
[16] N.S. Abdul Mubarak, et al., Immobilized Fe-loaded chitosan film for methyl orange dye removal: competitive ions, reusability, and mechanism, J. Polym. Environ. (2021) 29.
[17] G.Z. Kyzas, J. Fu, K.A. Matis, The change from past to future for adsorbent materials in treatment of dyeing wastewaters. Materials, Basel 6 (11) (2013) 5131–5158.
[18] T.M. Albayati, G.M. Alwan, O.S. Mahdy, High performance methyl orange capture on magnetic nanoporous MCM-41 prepared by incipient wetness impregnation method. Korean Journal of Chemical Engineering 34 (1) (2017) 259–265.
[19] T. Taweekarn, W. Wongniramaikul, A. Choodum, Removal and recovery of phosphate using a novel calcium silicate hydrate composite starch cryogel. Journal of Environmental Management 301 (2022) 113923.
[20] M. Mohd Nazri, N. Sapawe, Removal of methyl orange over low-cost silica nanoparticles extrated from bamboo leaves ash, Mater. Today: Proc. (2020) 31.
[21] D.F. Mohamad, et al., Synthesis of mesoporous silica nanoparticle from banana peel ash for removal of phenol and methyl orange in aqueous solution, Mater. Today: Proc. 19 (2019) 1119–1125.
[22] S. Ding, et al., Immobilization of powdery calcium silicate hydrate via PVA covalent cross-linking process for phosphorus removal, Sci. Total Environ. 645 (2018) 937–945.
[23] T. Taweekarn, et al., Starch biocryogel for removal of methylene blue by batch adsorption. Polymers, Basel 24 (2022) 14.
[24] Xinxin Yang, et al., One-step fabrication of chitosan-Fe(OH)3 beads for efficient adsorption of anionic dyes. International Journal of Biological Macromolecules 117 (2018) 30–41.

[25] C. Boonkanon, et al., Preparation and characterization of calcium cross-linked starch monolithic cryogels and their application as cost-effective green filters, Polymers, Basel 22 (2021) 13.

[26] S. Mallakpour, S. Rashidimoghadam, *Starch/MWCNT-vitamin C nanocomposites: electrical, thermal properties and their utilization for removal of methyl orange*, Carbohydrate Polymers 169 (2017) 23–32.

[27] T. Taweekarn, et al., Griess-doped polyvinyl alcohol thin film for on-site simultaneous sample preparation and nitrite determination of processed meat products, Food Chem. 389 (2022) 133085.

[28] T. Taweekarn, et al., *A novel colorimetric sensor based on modified mesoporous silica nanoparticles for rapid on-site detection of nitrite*, Mikrochim Acta 187 (12) (2020) 643.

[29] E.H. Mekatel, et al., Adsorption of methyl orange on nanoparticles of a synthetic zeolite NaA/CuO, Compt. Rendus Chem. 18 (3) (2015) 336–344.

[30] P. Zhao, R. Zhang, J. Wang, Adsorption of methyl orange from aqueous solution using chitosan/diatomite composite, Water Sci. Technol. 75 (7–8) (2017) 1633–1642.

[31] J. Goscianska, I. Nowak, A. Olejnik, Sorptive properties of aluminium ions containing mesoporous silica towards l-histidine, Adsorption (2016) 22.

[32] S. Kaewnoo, et al., Effective recovery of phosphate from wastewater using biodegradable calcium-rich shell wastes composite macroporous cryogel, Colloids Surf. A Physicochem. Eng. Asp. 691 (2024) 133857.

[33] C. Boonkanon, et al., Preparation and characterization of calcium cross-linked starch monolithic cryogels and their application as cost-effective green filters, Polymers 13 (22) (2021) 3975.

[34] C. Phawachalotorn, et al., Continuous phosphate removal and recovery using a calcium silicate hydrate composite monolithic cryogel column, Polymers 15 (3) (2023) 539.

[35] F. Ai, et al., Facile synthesis of cetyltrimethylammonium bromide-loaded mesoporous silica nanoparticles for efficient inhibition of hepatocellular carcinoma cell proliferation, Mater. Res. Express 7 (8) (2020) 85008.

[36] O. Osta, et al., Direct synthesis of mesoporous organosilica and proof-of-concept applications in lysozyme adsorption and supported catalysis, ACS Omega 5 (30) (2020) 18842–18848.

[37] Y. Mehmood, et al., Facile synthesis of mesoporous silica nanoparticles using modified sol-gel method: optimization and in vitro cytotoxicity studies, Pak. J. Pharm. Sci. (2019) 1805–1812, 32(4(Supplementary).

[38] A. Choodum, W. Sriprom, W. Wongniramaikul, Portable and selective colorimetric film and digital image colorimetry for detection of iron, Spectrochim. Acta Mol. Biomol. Spectrosc. 208 (2019) 40–47.

[39] A. Choodum, et al., Greener monolithic solid phase extraction biosorbent based on calcium cross-linked starch cryogel composite graphene oxide nanoparticles for benzo(a)pyrene analysis, Molecules 26 (20) (2021) 6163.

[40] S. Shawky, et al., Efficient Loading and Encapsulation of Anti-Tuberculosis Drugs using Multifunctional Mesoporous Silicate Nanoparticles Running Title: Mesoporous Silicate Nanoparticles as Smart Drug Delivery System. (2016) 11.

[41] D. Kalyani, et al., Biodegradation and detoxification of reactive textile dye by isolated Pseudomonas sp SUK1. Water environment research, a research publication of the Water Environment Federation 81 (2009) 298–307.

[42] A. Alfawaz, et al., Surface functionalization of mesoporous silica nanoparticles with brønsted acids as a catalyst for esterificatsion reaction. Journal of King Saud University - Science 34 (5) (2022) 102106.

[43] K. Chen, et al., Model construction of micro-pores in shale: a case study of Silurian Longmaxi Formation shale in Dianqianbei area, SW China. Petroleum Exploration and Development 45 (2018) 412–421.

[44] H. Sanaeishoar, M. Sabbaghan, F. Mohave, Synthesis and characterization of micro-mesoporous MCM-41 using various ionic liquids as co-templates, Microporous Mesoporous Mater. 217 (2015) 219–224.

[45] M.K. Kim, et al., Optimization of mesoporous silica nanoparticles through statistical design of experiment and the application for the anticancer drug, Pharmaceutics 2 (2021) 13.

[46] S. Chaudhary, D. Rohilla, S. Mehta, Surfactant adsorption and aggregate structure of silica nanoparticles: a versatile stratagem for the regulation of particle size and surface modification, Mater. Res. Express 1 (2014) 15011.

[47] X. Zhang, et al., Adsorption of methyl orange dye by SiO2 mesoporous nanoparticles: adsorption kinetics and eco-toxicity assessment in Zea mays sprout and Artemia salina. Environmental Science and Pollution Research 30 (55) (2023) 117000–117010.

[48] O.A. Saputra, et al., Organically surface engineered mesoporous silica nanoparticles control the release of quercetin by pH stimuli, Sci. Rep. 12 (1) (2022) 20661.

[49] L.G. Freidus, et al., Theranostic mesoporous silica nanoparticles loaded with a curcumin-naphthoquinone conjugate for potential cancer intervention, Front. Mol. Biosci. (2021) 8.

[50] T. Christoforidou, et al., Oral drug delivery systems based on ordered mesoporous silica nanoparticles for modulating the release of aprepitant. International journal of molecular sciences 22 (4) (2021) 1896.

[51] G.C. Carvalho, et al., Physicochemical characterization of a lycopene-loaded mesoporous silica nanoparticle formulation, Nano Select 5 (7–8) (2024) 2300131.

[52] C.M. Bryant, B.R. Hamaker, Effect of lime on gelatinization of corn flour and starch, Cereal Chem. 74 (2) (1997) 171–175.

[53] W. Chanjarujit, P. Hongsprabhas, S. Chaiseri, Physicochemical properties and flavor retention ability of alkaline calcium hydroxide-mungbean starch films, Carbohydrate Polymers (2018) 198.

[54] S.I. Raj, A. Jaiswal, I. Uddin, Tunable porous silica nanoparticles as a universal dye adsorbent, RSC Adv. 9 (20) (2019) 11212–11219.

[55] J. Pal, et al., Removal of methyl orange by activated carbon modified by silver nanoparticles, Appl. Water Sci. 3 (2) (2013) 367–374.

[56] M.C. Avila, et al., Adsorption of an anionic dye from aqueous solution on a treated clay. Groundwater for Sustainable Development 15 (2021) 100688.

[57] R. Lafi, A. Hafiane, Removal of methyl orange (MO) from aqueous solution using cationic surfactants modified coffee waste (MCWs). Journal of the Taiwan Institute of Chemical Engineers 58 (2016) 424–433.

[58] H.T. Hii, Adsorption isotherm and kinetic models for removal of methyl orange and remazol brilliant blue R by coconut shell activated carbon, Tropical Aquatic and Soil Pollution 1 (1) (2021) 1–10.

[59] S.S. Shah, et al., Adsorptive removal of methyl orange dye from aqueous solution using populous leaves: insights from kinetics, thermodynamics and computational studies. Environmental Chemistry and Ecotoxicology 3 (2021) 172–181.

[60] H. Li, et al., Magnetic Fe3O4@SiO2 study on adsorption of methyl orange on nanoparticles, Sci. Rep. 14 (1) (2024) 1217.

[61] M.A. Ahmad, N.A. Ahmad Puad, O.S. Bello, *Kinetic, equilibrium and thermodynamic studies of synthetic dye removal using pomegranate peel activated carbon prepared by microwave-induced KOH activation*, Water Resources and Industry 6 (2014) 18–35.

[62] Saruchi and V, Kumar, Adsorption kinetics and isotherms for the removal of rhodamine B dye and Pb+2 ions from aqueous solutions by a hybrid ion-exchanger, Arab. J. Chem. 12 (3) (2019) 316–329.

[63] A. Bhatnagar, et al., Removal of nitrate from water by adsorption onto zinc chloride treated activated carbon. Separation science and technology 43 (4) (2008) 886–907.

[64] Y. Yu, Y.-Y. Zhuang, Z.-H. Wang, *Adsorption of water-soluble Dye onto functionalized resin*. Journal of colloid and interface science 242 (2) (2001) 288–293.

[65] P.M. Birgani, et al., An efficient and economical treatment for batik textile wastewater containing high levels of silicate and organic pollutants using a sequential process of acidification, magnesium oxide, and palm shell-based activated carbon application. Journal of Environmental Management 184 (2016) 229–239.

[66] W.F. Wan Mohd Khalik, et al., Decolorization and mineralization of batik wastewater through solar photocatalytic process, Sains Malays. 44 (2015) 607–612.

[67] R. Haounati, et al., Elaboration and properties of a new SDS/CTAB@Montmorillonite organoclay composite as a superb adsorbent for the removal of malachite green from aqueous solutions. Separation and Purification Technology 255 (2021) 117335.

[68] S. Asuha, X.G. Zhou, S. Zhao, Adsorption of methyl orange and Cr(VI) on mesoporous TiO2 prepared by hydrothermal method, J. Hazard Mater. 181 (1) (2010) 204–210.

[69] R. Lafi, et al., Removal of methyl orange from aqueous solution onto modified extracted cellulose from Stipa Tenacissima L. International Journal of Environmental Analytical Chemistry 102 (19) (2022) 8124–8140.

[70] The Ministry of Natural Resources and Environment of Thailand, The Ministry of Natural Resources and Environment of Thailand, in: Notification of the Ministry of Natural Resources and Environment for Standard Levels for Discharge from Municipal Wastewater Treatment Plant, 2010.

[71] M.K. Uddin, U. Baig, *Synthesis of Co3O4 nanoparticles and their performance towards methyl orange dye removal: characterisation, adsorption and response surface methodology.* Journal of Cleaner Production 211 (2019) 1141–1153.

[72] F. Krika, O.e.F. Benlahbib, Removal of methyl orange from aqueous solution via adsorption on cork as a natural and low-coast adsorbent: equilibrium, kinetic and thermodynamic study of removal process. Desalination and Water Treatment 53 (13) (2015) 3711–3723.